Biomaterials 313 (2025) 122810

Contents lists available at ScienceDirect

Biomaterials

journal homepage: www.elsevier.com/locate/biomaterials

Epidermal secretion-purified biosensing patch with hydrogel sebum filtering membrane and unidirectional flow microfluidic channels

Yuqi Wang, Ziyu Zhang, Yuqing Shi, Xiong Yu, Xinyi Zhang, Xiaohao Ma, Junjie Su, Ruochen Ding, Yuanjing Lin *

School of Microelectronics, Southern University of Science and Technology, Shenzhen, 518055, China

ARTICLE INFO

Keywords:
Biosensors
Sebum filtering
Tesla valve
Microfluidic design
Sweat analysis

ABSTRACT

The development of biosensing electronics for real-time sweat analysis has attracted increasing research interest due to their promising applications for non-invasive health monitoring. However, one of the critical challenges lies in the sebum interference that largely limits the sensing reliability in practical scenarios. Herein, we report a flexible epidermal secretion-purified biosensing patch with a hydrogel filtering membrane that can effectively eliminate the impact of sebum and sebum-soluble substances. The as-prepared sebum filtering membranes feature a dual-layer sebum-resistant structure based on the poly(hydroxyethyl methacrylate) hydrogel functionalized with nano-brush structured poly(sulfobetaine) to eliminate interferences and provide self-cleaning capability. Furthermore, the unidirectional flow microfluidic channels design based on the Tesla valve was incorporated into the biosensing patch to prevent external sebum contamination and allow effective sweat refreshing for reliable sensing. By seamlessly combining these components, the epidermal secretion-purified biosensing patch enables continuous monitoring of sweat uric acid, pH, and sodium ions with significantly improved accuracy of up to 12 %. The proposed strategy for enhanced sweat sensing reliability without sebum interference shows desirable compatibility for different types of biosensors and would inspire the advances of flexible and wearable devices for non-invasive healthcare.

1. Introduction

The development of wearable biosensing systems has attracted enormous research interest in recent years due to the capability for dynamic and non-invasive monitoring of the epidermal biomarkers in sweat [1–6]. Epidermal secretions contain a variety of components, including sebum, sweat, and corneocyte debris [7,8]. Sebum is a lipid-rich fluid produced by the sebaceous glands, which is delivered into the sebaceous duct and then flows along the hair follicles to the skin surface [9]. The largest number of sebum glands are on the face, back, and upper chest, where the number of sebum glands is between 400 and 900/cm^2 [10,11]. In general, the sebum secretion rate varies from person to person between 0.05 and 0.4 mg/cm^2 per 3 h [12,13]. Studies have suggested that sebum or other lipids in epidermal secretion could introduce large interference to the biosensing performances, especially for the enzymatic and ion-selective sensors that were commonly used for real-time sweat analysis [14–18]. For instance, sebum tends to adsorb onto the sensor surface, forming a barrier at the interface to prohibit smooth ions/molecules transfer [19,20]. Also, the lipid components in sebum may competitively bind to lipophilic enzymes, which would occupy the binding sites of enzymes on sensors and even disrupt their protein structure [12,16,21,22]. Moreover, the permselective lipophilic ion exchangers supporting ion-selective electrodes may also suffer structural damage due to sebum accumulation [23–25]. Previous research aimed at sweat sensing with enhanced reliability has mainly focused on improving the sensor sensitivity, selectivity, and stability, as well as eliminating the interferences from pH values and temperatures [26–31]. However, effective sebum filtering for real-time epidermal analysis is less explored.

To achieve sebum filtering from sweat, one of the possible strategies is utilizing the water/oil separation properties of membranes based on Janus fibers and hydrogels [32–35]. Such membranes with rational surface functionalization can achieve in-situ sebum filtering [36,37]. For instance, with pore size manipulation and novel nano-architectures such as the nano-brush on the membranes, the sebum and other interference elements in relatively large sizes can be blocked [38,39].

* Corresponding author.
E-mail address: linyj2020@sustech.edu.cn (Y. Lin).

https://doi.org/10.1016/j.biomaterials.2024.122810
Received 15 June 2024; Received in revised form 22 August 2024; Accepted 2 September 2024
Available online 3 September 2024

Additionally, chemical agents are normally employed to realize super-hydrophilic or super-hydrophobic surfaces, thereby enhancing anti-pollution properties [40].

Meanwhile, microfluidic platforms with unidirectional flow properties can be utilized to establish efficient sweat sampling and refreshing without interference from remaining sweat [41]. Among various microfluidic designs, the Tesla valve, invented by Nikola Tesla in 1919, exhibits a distinctive construction whereby the pressure drops experienced by a fluid flowing forward through the valve is lower compared to that of a fluid flowing in reverse [42]. Thus, microfluidic channels based on the Tesla valve architectures can be utilized to realize the unidirectional flow of the epidermal sweat so as to improve the sensing accuracy and temporal resolution [43].

In this work, by integrating a hydrogel sebum filtering membrane and microfluidic channel based on the Tesla valve into a wearable sweat sensing patch, epidermal sweat analysis with significantly enhanced accuracy was demonstrated. The poly(vinylidene fluoride) (PVDF) microfiltration membranes were functionalized with hydrophilic hydrogel for effective sweat collection and polyzwitterionic nano-brush structures to facilitate the desorption of sebum. Therefore, the as-prepared membranes exhibit superior sweat/sebum separation and self-cleaning capabilities. The effectiveness of adopting such membranes for sweat sensing was validated in enzymatic uric acid (UA) sensing and selective ion sensing of pH and sodium (Na^+). By eliminating the interferences from sebum and other lipid elements, improved accuracy in the range of 7–12 % was observed with minimized signal fluctuation. In addition, the microfluidic channels designed with a double vein arc based on Tesla valves contributed to the unidirectional flow guiding of sweat, thus preventing potential biomarkers interferences from reverse flow. As a concept demonstration, the integrated epidermal secretion-purified biosensing patch with biosensors array for uric acid, pH, and Na^+ was applied for real-time sweat analysis during exercise. The sensing reliability was validated with standard analytical tools and delivered high consistency. The proposed strategy to enhance the accuracy of sweat biomarkers analysis by integration of secretion-purified membranes and unidirectional flow microfluidic design into the biosensing patch presents high promise for practical, non-invasive health monitoring applications.

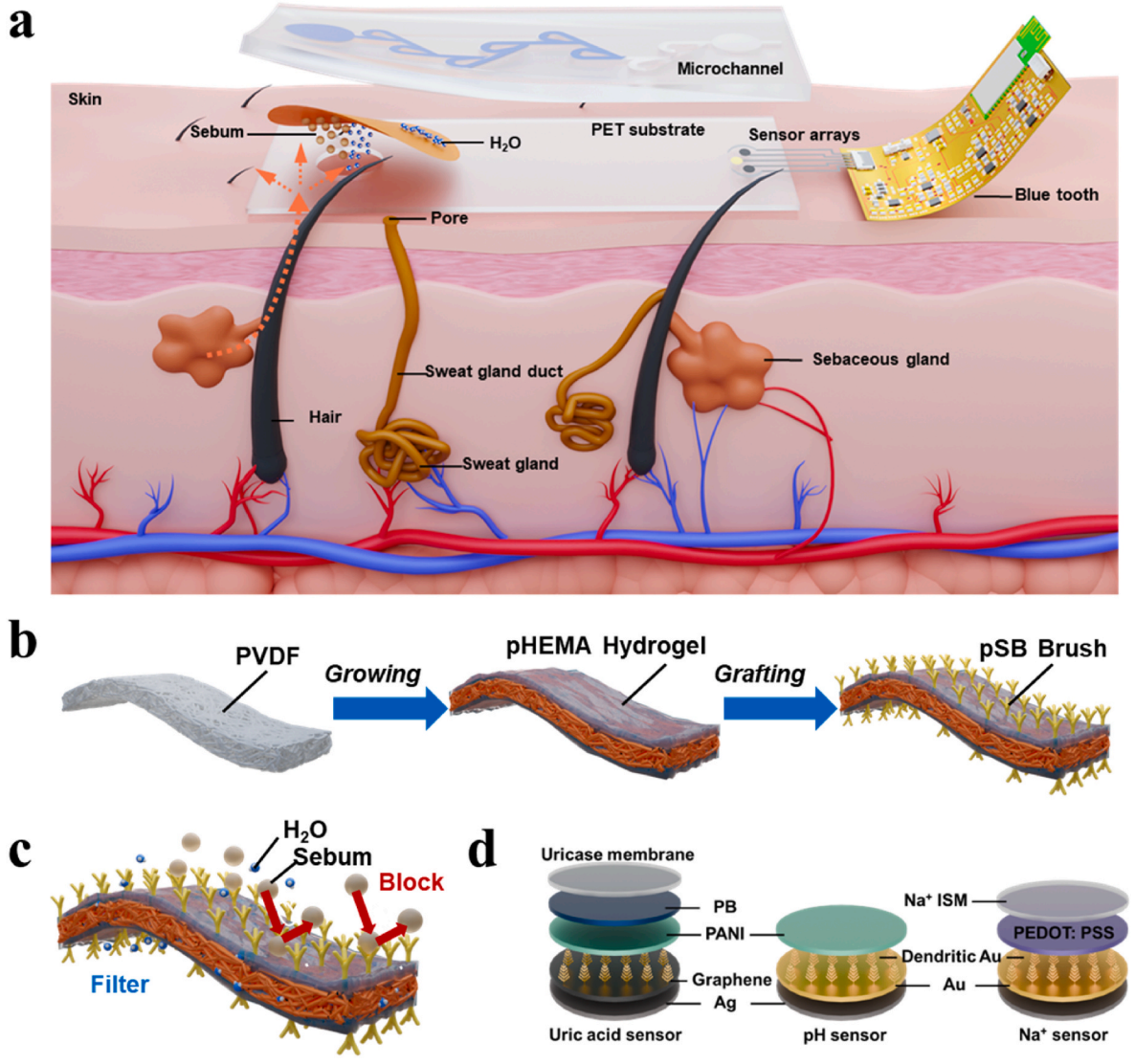

Fig. 1. Schematic illustration of the epidermal secretion-purified biosensing patch. (a) The sensing patch for sweat/sebum separation, sweat transportation in unidirectional flow microfluidic channels, and biosensing with wireless data transmission. (b) The fabrication process of the PVDF-pHEMA$_{gel}$-pSB$_{brush}$ membrane for sebum filtering. (c) The principle of sweat/sebum separation of the PVDF-pHEMA$_{gel}$-pSB$_{brush}$ membrane. (d) Layer-by-layer architectures of the electrochemical sensors for highly selective sensing of sweat uric acid, pH, and Na^+.

2. Result

2.1. Design and fabrication of epidermal secretion-purified biosensing patch

The epidermal secretion-purified biosensing patch mainly consists of the hydrogel membrane for sweat/sebum separation, PDMS unidirectional flow microfluidic channel based on the Tesla valve for sweat collection and transportation, highly selective sensor arrays constructed on flexible polyethylene terephthalate (PET) substrate for uric acid, pH, and Na^+ detection, and customed design circuit for wireless data transmission (Fig. 1a). As shown in Fig. 1b and Fig. S1, the poly(vinylidene fluoride) (PVDF) microfiltration membrane was first functionalized with a layer of poly(hydroxyethyl methacrylate) (pHEMA) hydrogel. The pHEMA hydrogel layer can significantly improve the hydrophilicity of the filtering membrane, prevent small particles in the secretion from clogging the holes on the PVDF microfiltration membrane, and isolate sebum from flowing through the membrane. The hydrogel layer on both sides was subsequently decorated with poly (sulfobetaine) (pSB) in a nano-brush structure to obtain the final PVDF-$pHEMA_{gel}$-pSB_{brush} membrane. The brush structure can further propel the sebum away from the filtering membrane [35]. Interestingly, the pSB brush would vertically spring up when immersed in liquid, thus desorbing the sebum residue on the hydrogel layer in a self-cleaning manner (Fig. 1c). The purified secretion can then pass through the PVDF-$pHEMA_{gel}$-pSB_{brush} membrane and flow through the microfluidic channel to the reservoir with an electrochemical sensors array. The layer-by-layer architectures of the sensors for highly selective sensing of sweat uric acid, pH, and Na^+ are displayed in Fig. 1d. The extracted sensing signals are transmitted through Bluetooth and displayed on a customed design mobile App to realize wireless physiological status tracking with enhanced reliability.

2.2. Characterizations of the hydrogel sebum filtering membrane

The hydrogel sebum filtering membranes exhibit desirable performance through chemical modification on the surface of PVDF microfiltration membranes. The functionalized chemical composites of the $pHEMA_{gel}$-pSB_{brush} double layers were characterized by Fourier transform infrared spectroscopy (FTIR) and X-ray photoelectron spectroscopy (XPS). As shown in Fig. 2a, the peak at 1726 cm^{-1} ascribing to C═O stretching vibration indicates the copolymerization of the PVDF-$pHEMA_{gel}$ membrane. The amination cross-linking of the PVDF-$pHEMA_{gel}$ membrane was then verified by the increasing N percentage and the peak at 1558 cm^{-1} belonging to the bending vibration of N–H (in-plane). Finally, the strong peaks at 1726, 1487, and 1038 cm^{-1} in the ATR-FTIR spectrum of the PVDF-$pHEMA_{gel}$-pSB_{brush} membrane were assigned to the C═O stretching vibration, C–N stretching vibration, and S═O symmetrical stretching vibration of pSB brushes, respectively. The element composition of the was further confirmed in the XPS spectra in Fig. 2b. As shown in the XPS spectra, compared with the PVDF membrane, the decrease of F and the increase of C, O, N, and P in the atomic percentage of the PVDF-$pHEMA_{gel}$-pSB_{brush} membrane directly proves the stepwise coverage of the PVDF substrate by the modification layer.

The as-prepared PVDF-$pHEMA_{gel}$-pSB_{brush} membranes retain highly porous network architectures on the surface after chemical functionalization. As shown in the SEM of Fig. 2c, the functionalized membranes present an asymmetrical microporous structure in 0.22 μm, which is

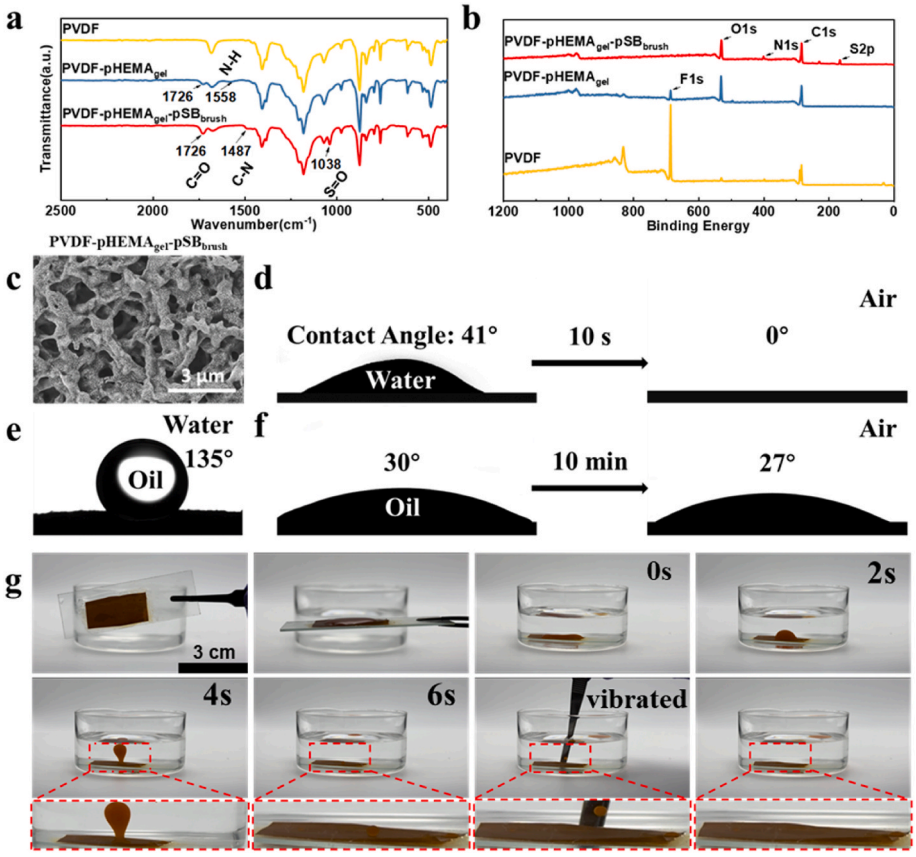

Fig. 2. Characterization of the surface properties of the PVDF-$pHEMA_{gel}$-pSB_{brush} membranes. (a) The FTIR and (b) XPS spectra of PVDF-$pHEMA_{gel}$-pSB_{brush} membranes before and after chemical modification. (c) SEM images of PVDF-$pHEMA_{gel}$-pSB_{brush} membrane. (d) Water contact angle in ambient. (e)–(f) The sebum contact angle under the water and ambient, respectively. (g) The self-cleaning capability of the PVDF-$pHEMA_{gel}$-pSB_{brush} membrane with residue sebum dyed in red. (For interpretation of the references to colour in this figure legend, the reader is referred to the Web version of this article.)

similar to the pristine PVDF microfiltration membrane surface morphology (Fig. S2). It ensures a smooth passway for sweat after sebum filtering. The wettability and oleophobic performance of the PVDF-pHEMA$_{gel}$-pSB$_{brush}$ membrane were evaluated by the water contact angle and underwater sebum contact angle, respectively. As shown in Fig. 2d, the initial water contact angle of the PVDF-pHEMA$_{gel}$-pSB$_{brush}$ membrane was around 41° and quickly decreased to 0° within 10 s, which indicates superior wettability. In Fig. 2e, the oleophobic property of the membrane can be confirmed from the large angle of 135° with a sebum droplet in water. Even though the hydrated membrane surface exhibited a sebum contact angle of 30° in the ambient, which is mainly due to surface tension within 24×10^{-3} and 9×10^{-3} N/m, it remains nearly unchanged after 10 min (Fig. 2f).

The PVDF-pHEMA$_{gel}$-pSB$_{brush}$ membranes, which have such wettability and oleophobic performance, enable attractive self-cleaning capabilities against sebum. Fig. 2g and Movie S1 show that the membrane with sebum residue dyed brown was first immersed in the water. The sebum quickly accumulates into a droplet and is propelled from the membrane surface. To further assess the self-cleaning capacity of the as-fabricated membrane in accumulated sebum, the membrane was kept 30° inclined and subjected to sweat-sebum simulated solution with a flow rate of 4 mL/min, simulating the process in practical scenarios where fluid might partially permeate through or flow over the membrane surface. The freeze-dried membranes, after testing, show a mass change of less than 0.4 mg (equivalent to around 0.3 μL), indicating that negligible sebum would accumulate on the membrane (Fig. S3). Such self-clean capability can be attributed to the polyzwitterionic nanobrush layer and indicates the practical application in sweat collection with effective sebum removals and reusability.

2.3. Performance evaluation of the electrochemical biosensors with the sebum filtering membrane

To evaluate the enhancement of biosensing reliability with the as-prepared hydrogel sebum filtering membrane, the sensing performances with or without sebum were compared. Three types of sensors, namely enzymatic uric acid sensors, ionophore-based Na^+ sensors, and pH sensors without biomaterial layers, were adopted for the systematic tests. As shown in Fig. 3a, the uric acid sweat sensor delivers a sensitivity of 5.44 μA/mM in the range of 12.5–100 μM in the standard solution. However, the sensing performance shows significant difference and non-linearity in a solution containing 137.5 μg/μL sebum. The mixture solution was then filtered with the membrane for the third-round test, and the sensitivity can be well recovered, as shown in Fig. 3c and d. It is worth mentioning that although the sensitivity of UA with sebum appears to be higher, the R^2 coefficient of the fitting equation is relatively low ($R^2 = 0.907$), and a large variation in the sensing range below 50 μM can be observed. This indicates that the presence of sebum introduces interference on the uric acid sensing. Similar results can be observed for the pH and Na^+ sensors. The pH sensor sensitivities with and without the membrane are 58.4 and 59.6 mV/dec, respectively (Fig. 3e and Fig. S3). The Na^+ sensors sensitivities with and without the membrane are 46.7 and 52.4 mV/dec, respectively, which proves that the membrane application achieves a 12 % improvement of sensitivity by ratio (Fig. 3f and Fig. S4). These indicate that the sebum also introduces fluctuations to the ionophore membranes and other active layers, which would result in relatively large variation, as shown in Fig. 3g and h. In the solution filtered with the membranes, the ion sensing sensitivities recovered to the equivalent values in the standard ones without sebum, which further validates the effectiveness of mitigating such sensing inaccuracy with the as-fabricated membranes.

2.4. Design and fabrication of the unidirectional flow Tesla valve microfluidic channels

Apart from sebum filtering, it is crucial to prevent cross-contamination within refreshing and sitting sweat in the flowing channels. Unidirectional flow guiding microfluidic channel based on the Tesla valve is one of the promising designs. It possesses low flow resistance in the forward direction and high resistance in the reverse direction. To prepare a flexible Tesla valve microfluidic channel patch for wearable sweat collection and transport, 3D printed transfer molding fabrication procedures were adopted, as illustrated in Fig. 4a and Fig. S5. The 3D printed mold with negative Tesla valve architectures was first cleaned with O_2 plasma, enhancing hydrophilicity. Thus, the PDMS coated on the mold can be peeled off smoothly with designed microfluidic structures. The as-prepared flexible microfluidic PDMS layer was bonded with the sensors via UV epoxy into an integrated sensing patch (Fig. 4b). The sweat collection capability of the microfluidic channels was evaluated with dye. As shown in Fig. 4c and Movie S2, a flow meter introduces liquid dyed in black into the device with 2 μL/s, which indicates that there is no reverse flow in the channel and a total fluid volume of 190 μL can be stored in the patch. Movie S3 demonstrates the unidirectional flow characteristic of the microfluidic channel, where an initial volume of chlorocyclohexane (dyed orange) is pre-injected into the module, providing a clear contrast with the subsequent black-dyed artificial sweat injection.

The unidirectional flow property based on laminar single-phase flow was further analyzed. Fig. 4d and e presents the simulation results with reverse flow in the microfluidic channels. Part of the fluid in the main flow passage enters the annular branch and diverts, and these tributaries become the resistance of the main flow passage at the end of the annular branch. Such a dual counteracting effect hinders the flow of the main passage. As indicated by the velocity vectors in Fig. 4e, the flow is diverted into mainstream and annular tributaries, as can be seen in Area 1. The channel expansion in Area 2 and the accompanying flow collision in Area 3 result in pressure loss. Considering the channel area size, the design with 8 T valves was selected based on its capability to produce a relatively lower average velocity in the reversed flow from outlet to inlet, so as to realize unidirectional flow (Fig. S7). Therefore, such reverse flow would be inhibited, and the unidirectional forwarded flow can be realized, which plays a critical role in eliminating sweat sample interference during real-time monitoring.

2.5. On-body sweat analysis with the secretion-purified biosensing patch

To achieve real-time and wireless sweat analysis, the as-fabricated sebum filtering membrane and unidirectional flow microfluidic channel were integrated with the sensors array and a custom-designed flexible circuit for wireless signal transmission (Fig. 5a and Figure S6, S7). As shown in Fig. 5b, the signals of the biosensor will be processed by signal filtering and amplification before analog-to-digital conversion. The signals will be wirelessly transmitted by Bluetooth to the custom-designed mobile app for visualization of the sweat uric acid, pH, and Na^+ levels in real time (Movie S4). As a proof of concept, the integrated biosensing patch was worn on the volunteer's arm for epidermal sweat monitoring during cycling exercise (Fig. 5c). It should also be noted that to evaluate the effectiveness of secretion purification with the as-developed biosensing patch, skin pre-cleaning was not conducted to remove dermal residues from daily life and sebum. The sensors were calibrated with artificial sweat before on-body testing to ensure their sensing reliability (Fig. S8). After warming up for 20 min, the bio-signal extraction was activated for another 20 min, continuous tracking of sweat uric acid, pH, and Na^+ levels (Fig. 5d). The concentration of the uric acid, pH, and Na^+ extracted from the epidermal secretion-purified biosensing patch were further validated by LCMS, pH meter, and ICP-MS, respectively (Fig. 5e). The average errors of pH, Na^+, and uric acid sensors compared with standard analytical tools were 7.01 %, 9.25 %, and 16.67 %, respectively. The overall trends of the sweat biomarker concentrations extracted with the integrated patch align with the validation results, indicating enhanced reliability.

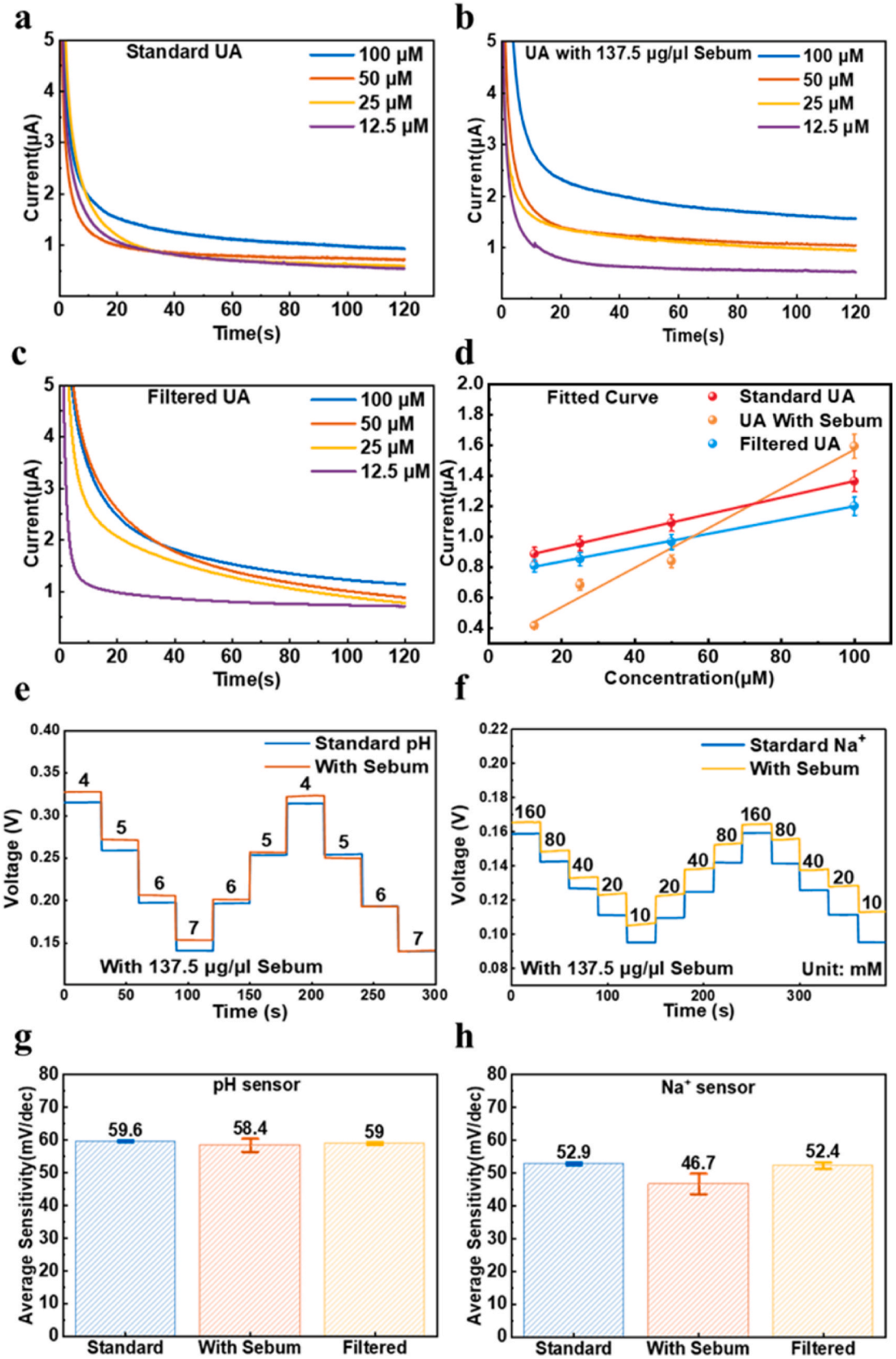

Fig. 3. Performance evaluation of the biosensor arrays with the hydrogel sebum filtering membrane. Uric acid sensor performance is (a) without sebum, (b) with sebum, and (c) with sebum filtering membrane. (d) Sensitivities of the uric acid sensors in three different solutions. (e) pH sensor and (f) Na^+ sensor performance with and without sebum. The average sensitivities and variations of five testing cycles of (g) pH sensor and (h) Na^+ sensor over three different solutions.

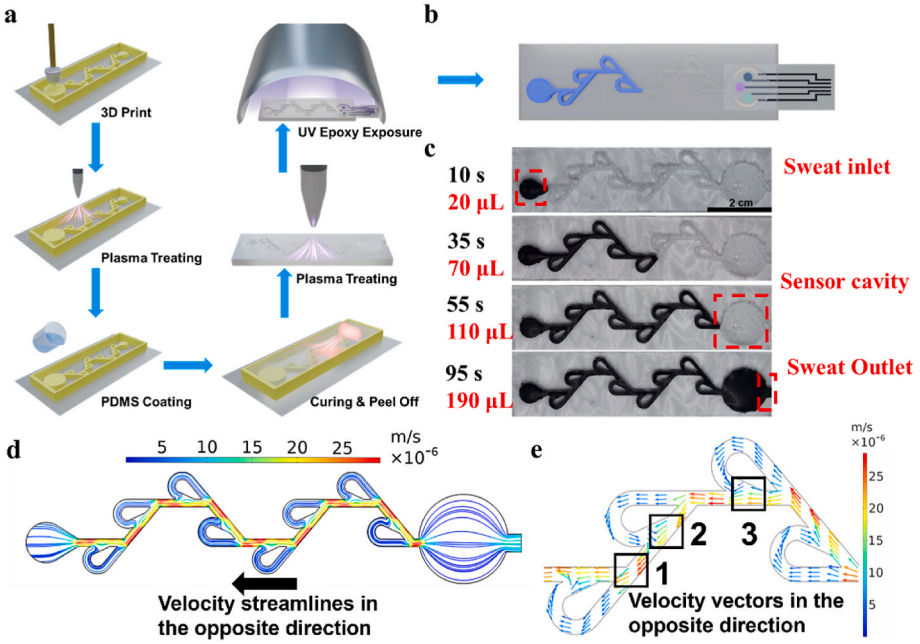

Fig. 4. The unidirectional flow microfluidic channel based on the Tesla valve design. (a) The fabrication process of microfluidic channels. (b) The encapsulation of the microfluidic channels. (c) The flow meter introduces liquid into the device, delivering volumes of 20 μL, 70 μL, 110 μL and 190 μL respectively. (d) The simulation results of the channel velocity streamlines. (e) Simulation results of the flow velocity vector in a reversed direction.

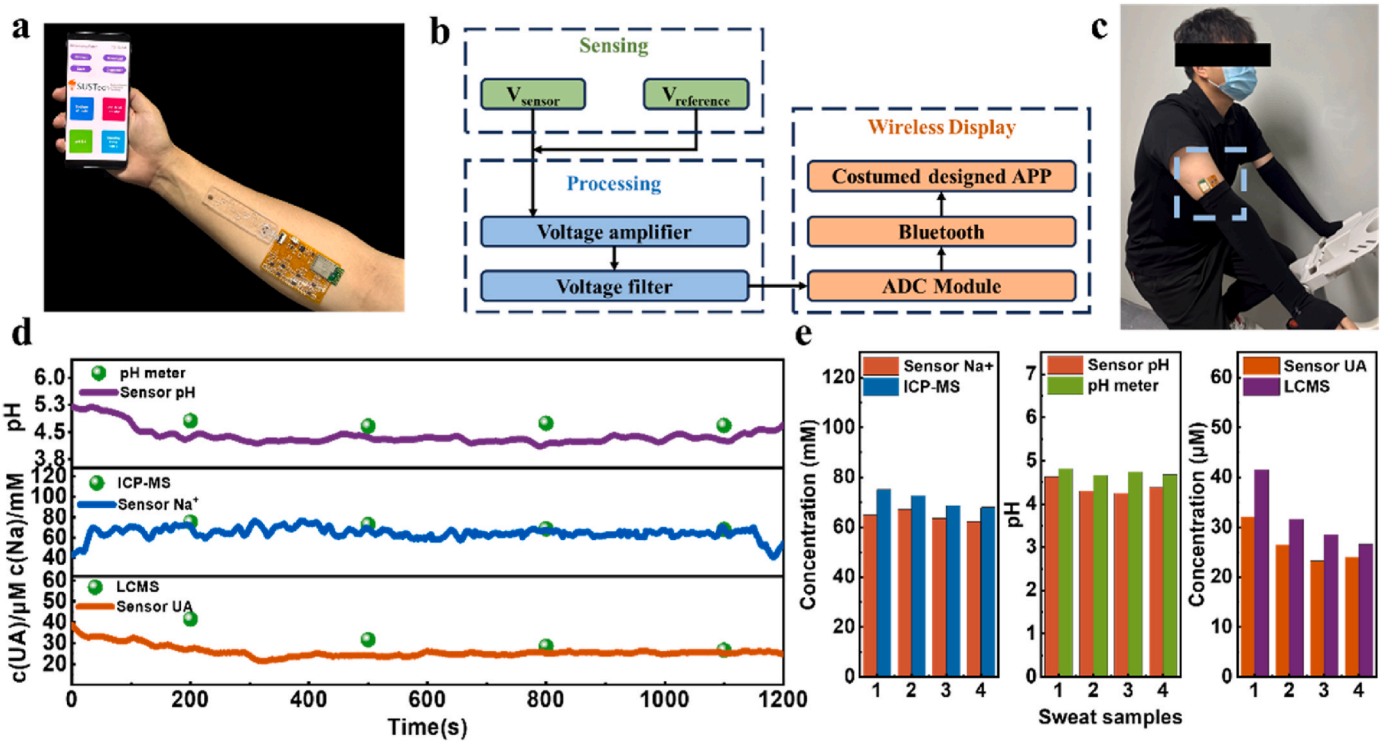

Fig. 5. On-body sweat sensing with the wearable epidermal secretion-purified biosensing patch. (a) Photograph of the wearable patch and the custom-designed mobile application for real-time and continuous sweat pH, Na^+, and uric acid sensing. (b) Schematic of signal processing and wireless transmission circuit design. (c) Photograph showing in-situ sweat monitoring with the wearable patch during exercise. (d) Real-time monitoring of sweat pH, Na^+, and uric acid levels during stationary cycling. (e) Comparison of the extracted pH, Na^+, and uric acid concentrations by the wearable patch and the validated results via analytical tools.

3. Conclusions

Wearable biosensing systems based on electrochemical sensors provide promising platforms for the non-invasive physiological monitoring of epidermal sweat. However, one of the challenges for sweat biosensing lies in epidermal secretion interference, such as sebum. In this work, a flexible biosensing patch that is capable of epidermal secretion purification was designed and fabricated. The interferences of sebum and sebum-soluble substances can be effectively eliminated with the integrated hydrogel filtering membrane at the sweat inlet. The as-fabricated

PVDF-pHEMA$_{gel}$-pSB$_{brush}$ sebum-resistant membrane can efficiently separate sebum from sweat samples and has self-cleaning properties. In addition, integrated microfluidic channels with unidirectional flow characteristics allow effective sweat refreshing and prevent sweat cross-contamination so as to further improve the continuous sensing accuracy. The integrated epidermal secretion-purified biosensing patch achieved improved accuracy of up to 12 % for uric acid, pH, and sodium ions monitoring, which indicates the combability for both enzymatic and selective ion sensing. The on-body sweat sensing reliability was also demonstrated by on-body sweat analysis during cycling exercise, and the results were validated with analytical tools. Such a rationally designed biosensing system that enables secretion purification provides a promising strategy to achieve enhanced accuracy and reliability for non-invasive health monitoring via epidermal sweat.

4. Experimental Section

4.1. Materials

Sodium hydroxide (NaOH), Sodium chloride (NaCl), Potassium chloride (KCl), Iron(III) chloride ($FeCl_3$), Tetrahydrofuran (THF), Polyvinyl butyral (PVB), Poly(vinyl chloride) (PVC), Ethanol, TEMED, Agarose, α-Bromoisobutyryl Bromide (BIBB), EDC-HCl, Copper(II) Bromide ($CuBr_2$), 2-Hydroxyethyl methacrylate (HEMA), MES monohydrate, 3,4-Ethylenedioxythiophene (EDOT), Ammonium persulfate (APS), Poly(sodium 4-styrene sulfonate) (NaPss), Na-TFPB, DMAPS, pyridine and N-Hydroxy succinimide (NHS) were purchased from Macklin. PVDF microfiltration membrane was purchased from F&H Technology. PDMS (SYLGARD 184) was purchased from the DOW chemical company. Sodium ionophore X, Potassium hexacyanoferrate (III) ($K_3[Fe(CN)_6]$), Gold(III) chloride hydrate, Nickel(II) nitrate hexahydrate, Aniline, Uricase, Prussian Blue, Bis(2-ethylhexyl) Sebacate (DOS), L-Ascorbic acid (L-AA), 2,2′-Bipyridyl (bpy) were purchased from Sigma-Aldrich. Hydrochloric acid was purchased from Dongjiang chemical reagent. Artificial sebum was purchased from Phygene Scientific. UV Epoxy was purchased from Shenzhen Longhesheng Technology.

4.2. Preparation of PVDF-pHEMA$_{gel}$-pSB$_{brush}$ membrane

As shown in Figure S1, 1.60 g of NaOH was dissolved in 80 mL of anhydrous ethanol at ambient temperature and subsequently heated to 80 °C. The PVDF microfiltration membrane was immersed for 15 s at this temperature, followed by a sequential rinsing with deionized (DI) water and ethanol. After air-drying at 60 °C, an alkali-treated PVDF-Alkenyl membrane was procured.

In a sealed environment, 5.86 g (45 mmol) of HEMA and 1.08 g (15 mmol) of AA were dissolved in a 40 mL solution comprising equal volumes of DI water and ethanol. The dried PVDF-Alkenyl membrane was immersed in this mixture, to which 0.68 g (3 mmol) of APS and 0.35 g (3 mmol) of TEMED were added. The container was sealed and maintained at room temperature, then the mixture was stirred at 60 °C and halted after 4 h. The resulting membrane was cleansed with ethanol and water to eliminate unbound polymers.

To further modify the membrane, 7.67 mg (0.04 mmol) of EDC-HCl and 11.51 mg (0.1 mmol) of NHS were dissolved in 20 mL of 10 mm MES buffer (pH 6.0). The membrane was submerged in this solution for 1 h at room temperature, followed by a gentle rinse with DI water. Subsequently, the PVDF-pHEMA$_{gel}$ membrane was immersed in a 20 mL solution of 10 mm PBS (pH 7.4) at room temperature for an additional 12 h.

The moist PVDF-pHEMA$_{gel}$ membrane was then stirred in excess THF for 1 h to remove surface residual water. It was later immersed in 25 mL of THF containing 0.79 g (10 mmol) of pyridine. A solution of 2.30 g (10 mmol) of BIBB in 15 mL of THF was gradually added to the mixture under stirring at 0 °C. The reaction was maintained at 0 °C for 2 h and then at room temperature for 12 h. After a wash with ethanol and water, the membrane was thoroughly soaked in water, prepping it for the next phase.

For the final modification, 0.70 g of DMAPS, 0.56 mg of CuBr2, 1.60 mg of bpy, and 26.42 mg of L-AA were dissolved in a 30 mL mixture of DI water and ethanol in a Schlenk tube. The prepared membrane was submerged in this solution, and the container was sealed. The mixture was stirred at 60 °C for 12 h. Following repeated rinsing with DI water, the final PVDF-pHEMA$_{gel}$-pSB$_{brush}$ membrane was soaked in excess DI water to replace the internal ethanol.

4.3. Long-term measurement of the membrane mass with the sebum-sweat simulated solution

A simulated solution was prepared by uniformly mixing 137.5 μg/μL of sebum with artificial sweat. The filter membrane was sealed and attached to a 30° inclined plane with holes. A fluid circulation system was set up using a peristaltic pump, allowing the simulated solution to flow uniformly over the filter membrane at a 4 mL/min rate. The membrane was then thoroughly dried, and weighed without any cleaning operation. This procedure was repeated every hour.

4.4. Preparation of the biosensing array

The sensor electrodes were prepared by printing conductive silver (Ag) ink on PET substrates. To achieve a large surface area, the Ag electrode patterns were texturized with Au nano-dendritic structures in the electrolyte with a mixture of 50 mM $HAuCl_4$ and 50 mM HCl. The deposition was conducted by applying a periodic voltage wave with an amplitude of −2 V, frequency of 50 Hz, and duty cycle of 50 % in gold planting solution for 3000 cycles. However, an electrode with Ag/AgCl ink covered with a Cl-saturated PVB membrane (same as the solution for the Na reference electrode) serves as the reference electrode.

For sodium ion sensors, the PEDOT: PSS was chosen as the ion-electron transducer and deposited onto the working electrodes. The electrolyte contains 10.6 μL EDOT, 206 mg NaPss, and 36.8 mg $K_3[Fe(CN)_6]$ in 10 mL DI. PEDOT deposition was realized under a periodic voltage wave with an amplitude of 0.865 V (DC offset at 0. 665V with amplitude of 0.2 V), frequency of 1 Hz, duty cycle of 25 % for 840 cycles in a fresh electrolyte containing. The electrode was then dried in the ambient, and 10 μL of the ion-selective membrane was drop cast on it. The Na^+ selective membrane cocktail consisted of Na ionophore X (1 % weight by weight, w/w), Na-TFPB (0.55 % w/w), PVC (33 % w/w), and DOS (65.45 % w/w). 100 mg of the membrane cocktail was dissolved in 660 μL of tetrahydrofuran. The ion-selective solutions were sealed and stored at 4 °C. The solution for the PVB reference electrode was prepared by dissolving 79.1 mg PVB and 50 mg of NaCl into 1 mL methanol. Ion-selective membranes were then prepared by drop-casting 10 μL of the Na^+ selective membrane cocktail on the working electrode 3 times. The reference electrode was modified by casting 10 μL of reference solution onto the Ag/AgCl electrode. The sensor was then left in the ambient overnight to dry and conditioned in 120 mM NaCl for 4 h before characterization.

For the pH sensors and uric acid sensors, PANI deposition was realized under a periodic voltage wave with an amplitude of 0.9 V, frequency of 1 Hz, and duty cycle of 10 % for 1200 cycles in a fresh electrolyte containing 0.1 M distilled aniline in 1 M HCl. The pH sensor electrode was then dried in the ambient and was stabilized in pH 5 buffer solution for 20 min before use. Continue for the uric acid sensors, Prussian blue (PB) deposition was realized under a periodic voltage wave (Gamry) with an amplitude of 0.5 V, frequency of 1 Hz, and duty cycle of 10 % for 60 cycles in a fresh electrolyte containing 2.5 mM $FeCl_3$ and 2.5 mM $K_3[Fe(CN)_6]$ in the supporting solution. The supporting solution is a mixture of 0.1 M KCl and 0.1 M HCl. The NiHCF layer, which serves to stabilize PB, was then deposited via CV scanning deposition with a potential window of 0–0.8V at a scan rate of 100 mV/s for 10 cycles in a fresh electrolyte containing 1 mM $Ni(NO_3)_2$ and 0.5

mM $K_3[Fe(CN)_6]$ in 1 M KCl. Emulsions for bulk agarose membranes contain 1 wt % agarose. 1 mg uricase powder was firstly dissolved in 100 μL PBS (pH 7.2), and the as-prepared enzymatic solution was mixed with membrane emulsion in a volume ratio of 1:2. 1 μL of the emulsion was then drop-cast onto the electrode and dried in the ambient environment. The solutions/emulsions were stored at 4 °C when not in use.

4.5. Performance evaluation of the electrochemical biosensors

The relative composition of sebum is 30–50 % triacylglycerols or diacylglycerols, 15–30 % free fatty acids, 12–20 % squalene, 26–30 % wax esters, 3–6% cholesterol esters, and 1.5–2.5 % cholesterol [12]. By using Liquid Chromatography Mass Spectrometer (LCMS) technology to quantify cholesterol content in collected sweat samples, we calculated an average sebum concentration of 145 μg/μL for this subject. Based on the average sebum concentration, three sets of solutions of the same sebum gradient were used for the experiment. The first set of solutions is the standard solution, and the second set of solutions is based on the first set of solutions to add sebum to simulate real sweat samples. The third set solution is the filtered solution of the second solution after membrane filtration. The sensor array prepared using the same process will first be validated using the first set of standard solutions. Then, 20 μL of the second and third sets of solution were added successively, and 5 test cycles were performed with gradient.

4.6. Fabrication of the microfluidic channel

The template of the microfluidic channel made of PLA was printed using a 3D printer (Creality K1) at a speed of 60 mm/s and treated with plasma. PDMS was homogeneously mixed at a 10:1 wt ratio of base to curing agent and placed in the vacuum hood for 30 min to remove small bubbles. Next, the PDMS was injected into the template and solidified at 60 °C in a high-temperature oven for 4 h. The cured PDMS with the microfluidic pattern was then peeled from the template and attached to the PET with sensor arrays to form microfluidic channels. The other side of the PET was attached to the double-sided medical tape. Thus, the microfluidic channel can adhere to the skin.

4.7. Simulation of the microfluidic channel

Comsol software was used to simulate the velocity of our design. A laminar flow model was adopted. Set all solid lines in the microfluidic channel model to be walls. The simulation model is super refined, and the entity is generated. The working conditions were set as 9.8 m/s^2 gravitational acceleration, 1-atm pressure, and 293.15 K for reference temperature. For test fluid properties, set the density (ρ) to 998.2 kg/m^3 and the dynamic viscosity (μ) to 0.001003 Pa s. The normal flow rate of test fluid at the entrance was set at 10^{-5} m/s with a volume fraction of 100 %, and the volume fraction of sweat at initialization was 0 %. With the set parameters, the flow rate on the channel was calculated. After the flow rate convergence test, the fluid simulation can provide information about the flow of sweat in the device and the distribution of physical quantities, such as velocity vectors based on the laminar flow model.

4.8. Sweat sampling experiments

All experiments were performed according to the university guidelines (The Ethics Guidelines for Research Involving Human Subjects or Human Tissue from Southern University of Science and Technology, SUSTech Institutional Review Board, 2024PES106). On-body evaluation of sweat analysis was performed on healthy volunteers aged between 20 and 26 years. For samples used for LCMS quantification of sebum concentration in sweat, volunteers were asked to undergo a sauna. After entering the sauna for 10 min and waiting for the volunteers to sweat fully, continue to collect sweat from their arms and chest areas. A batch of samples is made every 20 min. The collected samples were placed in an environment of 2–8 °C and then subjected to LCMS testing. For the on-body test, volunteers were asked to wear a sensing patch and sleeves and run on the treadmill to preheat for 20 min. After the sweat is filled in the channel, the volunteers engage in 20 minute stationary cycling while initiating signal transmission. Collect sweat from participants synchronously every 5 min for subsequent ICP-MS testing.

4.9. Characterization of the sweat samples

The sebum content is calculated by quantifying cholesterol in sweat samples using LCMS, and the proportion of cholesterol in sebum is 1.5–2.5 %. The liquid chromatography instrument is Ultimate 3000 UHPLC, and the chromatographic column is C18 (1.9 μm. 2.1 mm × 100 mm). The analysis uses a flow rate of 0.25 ml/min and an injection volume of 10 μL. The mobile phase uses 10 mM ammonium acetate 6:4 v/v ACN/H2O (A) −10 mM ammonium acetate 9:1 v/v IPA/ACN (B). The gradient elution procedure of the solution can be found in Supplementary Information 6. The mass spectrometer is a Q-Exactive (Thermo Fisher Scientific, CA, USA) HESI source. The ion source temperature is 310 °C, the capillary temperature is 320 °C, the sheath gas flow rate is 30 units, the auxiliary gas flow rate is 10 units, and the positive ion mode spray voltage is 3 kV. The analysis adopts Data Dependent Scanning Analysis (DDA), with a loop count set at 10 and a step-wise normalized collision energy set at 10, 28, and 35 eV for HCD energy. The scanning range of the primary mass spectrometry is 80–1200 *m/z*, with a resolution of 70000, AGC target set to 3×10^6, and injection time set to 200 ms. The resolution of the secondary mass spectrometry is set to 17500, the AGC target is set to 1×10^5, and the injection time is set to 50 ms. LCMS data was extracted from cholesterol peaks using Compound Discover software (V 3.2, Thermo Fisher Scientific, CA, USA) and then plotted using chromatographic peak area versus concentration.

The sweat samples obtained through on-body testing were measured using a pH meter (Sartorius PB-10). Measure each sample three times and take the average value. Use Agilent 7700 to quantify sodium concentration in sweat samples. Uptake time is 45 s, stabilization time is 30 s, and integer time per mass is 0.9 s.

Funding

This work was supported by the National Natural Science Foundation of China (62201243), Shenzhen Science and Technology Program (RCYX20231211090432060) and Shenzhen Stable Support Plan Program for Higher Education Institutions Research Program (20220815153728002).

Data and materials availability

All data needed to evaluate the conclusions in the paper are present in the paper and/or the Supplementary Materials.

CRediT authorship contribution statement

Yuqi Wang: Writing – review & editing, Writing – original draft, Visualization, Validation, Software, Resources, Project administration, Methodology, Investigation, Formal analysis, Data curation, Conceptualization. **Ziyu Zhang:** Methodology, Investigation, Data curation. **Yuqing Shi:** Writing – review & editing, Methodology. **Xiong Yu:** Methodology, Investigation. **Xinyi Zhang:** Methodology, Investigation. **Xiaohao Ma:** Writing – review & editing, Methodology. **Junjie Su:** Visualization, Software. **Ruochen Ding:** Methodology. **Yuanjing Lin:** Writing – review & editing, Supervision, Funding acquisition, Conceptualization.

Declaration of competing interest

The authors declare that they have no known competing financial

interests or personal relationships that could have appeared to influence the work reported in this paper.

Data availability

Data will be made available on request.

Acknowledgments

The authors would like to acknowledge the technical support from SUSTech CRF.

Appendix A. Supplementary data

Supplementary data to this article can be found online at https://doi.org/10.1016/j.biomaterials.2024.122810.

References

[1] C. Shi, Z. Zou, Z. Lei, P. Zhu, W. Zhang, J. Xiao, Heterogeneous integration of rigid, soft, and liquid materials for self-healable, recyclable, and reconfigurable wearable electronics, Sci. Adv. 6 (2020) eabd0202, https://doi.org/10.1126/sciadv.abd0202.

[2] N. Davis, J. Heikenfeld, C. Milla, A. Javey, The challenges and promise of sweat sensing, Nat. Biotechnol. (2024), https://doi.org/10.1038/s41587-023-02059-1.

[3] C. Xu, Y. Song, J.R. Sempionatto, S.A. Solomon, Y. Yu, H.Y.Y. Nyein, R.Y. Tay, J. Li, W. Heng, J. Min, A. Lao, T.K. Hsiai, J.A. Sumner, W. Gao, A physicochemical-sensing electronic skin for stress response monitoring, Nat Electron 7 (2024) 168–179, https://doi.org/10.1038/s41928-023-01116-6.

[4] S. Ma, Z. Wan, C. Wang, Z. Song, Y. Ding, D. Zhang, C.L.J. Chan, L. Shu, L. Huang, Z. Yang, F. Wang, J. Bai, Z. Fan, Y. Lin, Ultra-sensitive and stable multiplexed biosensors array in fully printed and integrated platforms for reliable perspiration analysis, Adv. Mater. 2311106 (2024), https://doi.org/10.1002/adma.202311106.

[5] L. Yin, M. Cao, K.N. Kim, M. Lin, J.-M. Moon, J.R. Sempionatto, J. Yu, R. Liu, C. Wicker, A. Trifonov, F. Zhang, H. Hu, J.R. Moreto, J. Go, S. Xu, J. Wang, A stretchable epidermal sweat sensing platform with an integrated printed battery and electrochromic display, Nat Electron 5 (2022) 694–705, https://doi.org/10.1038/s41928-022-00843-6.

[6] X. Ma, P. Wang, L. Huang, R. Ding, K. Zhou, Y. Shi, F. Chen, Q. Zhuang, Q. Huang, Y. Lin, Z. Zheng, A monolithically integrated in-textile wristband for wireless epidermal biosensing, Sci. Adv. 9 (2023) eadj2763, https://doi.org/10.1126/sciadv.adj2763.

[7] P. Wang, X. Ma, Z. Lin, F. Chen, Z. Chen, H. Hu, H. Xu, X. Zhang, Y. Shi, Q. Huang, Y. Lin, Z. Zheng, Well-defined in-textile photolithography towards permeable textile electronics, Nat. Commun. 15 (2024) 887, https://doi.org/10.1038/s41467-024-45287-y.

[8] S.R. Krishnan, T.R. Ray, A.B. Ayer, Y. Ma, P. Gutruf, K. Lee, J.Y. Lee, C. Wei, X. Feng, B. Ng, Z.A. Abecassis, N. Murthy, I. Stankiewicz, J. Freudman, J. Stillman, N. Kim, G. Young, C. Goudeseune, J. Ciraldo, M. Tate, Y. Huang, M. Potts, J. A. Rogers, Epidermal electronics for noninvasive, wireless, quantitative assessment of ventricular shunt function in patients with hydrocephalus, Sci. Transl. Med. 10 (2018) eaat8437, https://doi.org/10.1126/scitranslmed.aat8437.

[9] D.K. Trivedi, E. Sinclair, Y. Xu, D. Sarkar, C. Walton-Doyle, C. Liscio, P. Banks, J. Milne, M. Silverdale, T. Kunath, R. Goodacre, P. Barran, Discovery of volatile biomarkers of Parkinson's disease from sebum, ACS Cent. Sci. 5 (2019) 599–606, https://doi.org/10.1021/acscentsci.8b00879.

[10] Y. Liu, W. Jiang, Y. Tang, Q. Zhang, Y. Zhen, X. Wang, W. Liu, J. Wang, Y. Ma, Y. Tan, An optimal method for quantifying the facial sebum level and characterizing facial sebum features, Skin Res. Technol. 29 (2023) e13454, https://doi.org/10.1111/srt.13454.

[11] Z. Leng, P. Zhu, X. Wang, Y. Wang, P. Li, W. Huang, B. Li, R. Jin, N. Han, J. Wu, Y. Mao, Sebum-membrane-Inspired protein-based bioprotonic hydrogel for artificial skin and human-machine merging interface, Adv. Funct. Mater. 33 (2023) 2211056, https://doi.org/10.1002/adfm.202211056.

[12] C. Géhin, J. Tokarska, S.J. Fowler, P.E. Barran, D.K. Trivedi, No skin off your back: the sampling and extraction of sebum for metabolomics, Metabolomics 19 (2023) 21, https://doi.org/10.1007/s11306-023-01982-3.

[13] M. Ludovici, N. Kozul, S. Materazzi, R. Risoluti, M. Picardo, E. Camera, Influence of the sebaceous gland density on the stratum corneum lipidome, Sci. Rep. 8 (2018) 11500, https://doi.org/10.1038/s41598-018-29742-7.

[14] Y. Lin, M. Bariya, H.Y.Y. Nyein, L. Kivimäki, S. Uusitalo, E. Jansson, W. Ji, Z. Yuan, T. Happonen, C. Liedert, J. Hiltunen, Z. Fan, A. Javey, Porous enzymatic membrane for nanotextured glucose sweat sensors with high stability toward reliable noninvasive health monitoring, Adv Funct Materials 29 (2019) 1902521, https://doi.org/10.1002/adfm.201902521.

[15] R. Ghaffari, D.S. Yang, J. Kim, A. Mansour, J.A. Wright, J.B. Model, D.E. Wright, J. A. Rogers, T.R. Ray, State of sweat: emerging wearable systems for real-time, noninvasive sweat sensing and analytics, ACS Sens. 6 (2021) 2787–2801, https://doi.org/10.1021/acssensors.1c01133.

[16] M. Liu, G. Zhao, C. Yang, H. Wang, J. Cheng, An enzymatic electrochemical biosensing interface developed by the laser-induced graphene electrode, Adv Materials Inter 10 (2023) 2300235, https://doi.org/10.1002/admi.202300235.

[17] Y. Zhu, J. Li, J. Kim, S. Li, Y. Zhao, J. Bahari, P. Eliahoo, G. Li, S. Kawakita, R. Haghniaz, X. Gao, N. Falcone, M. Ermis, H. Kang, H. Liu, H. Kim, T. Tabish, H. Yu, B. Li, M. Akbari, S. Emaminejad, A. Khademhosseini, Skin-interfaced electronics: a promising and intelligent paradigm for personalized healthcare, Biomaterials 296 (2023) 122075, https://doi.org/10.1016/j.biomaterials.2023.122075.

[18] X. Zeng, R. Peng, Z. Fan, Y. Lin, Self-powered and wearable biosensors for healthcare, Mater. Today Energy 23 (2022) 100900, https://doi.org/10.1016/j.mtener.2021.100900.

[19] C. Li, L. Ren, C. Zhang, W. Xu, X. Liu, TiO2 coated polypropylene membrane by atomic layer deposition for oil–water mixture separation, Adv. Fiber Mater. 3 (2021) 138–146, https://doi.org/10.1007/s42765-021-00069-9.

[20] D. Teng, T. Zhao, Y. Xu, X. Zhang, Y. Zeng, The zein-based fiber membrane with switchable superwettability for on-demand oil/water separation, Separation and Purification Technology 263 (2021) 118393, https://doi.org/10.1016/j.seppur.2021.118393.

[21] M. Spick, K. Longman, C. Frampas, H. Lewis, C. Costa, D.D. Walters, A. Stewart, M. Wilde, D. Greener, G. Evetts, D. Trivedi, P. Barran, A. Pitt, M. Bailey, Changes to the sebum lipidome upon COVID-19 infection observed via rapid sampling from the skin, EClinicalMedicine 33 (2021) 100786, https://doi.org/10.1016/j.eclinm.2021.100786.

[22] M. Qin, H. Guo, Z. Dai, X. Yan, X. Ning, Advances in flexible and wearable pH sensors for wound healing monitoring, J. Semicond. 40 (2019) 111607, https://doi.org/10.1088/1674-4926/40/11/111607.

[23] Y. Shi, Z. Zhang, Q. Huang, Y. Lin, Z. Zheng, Wearable sweat biosensors on textiles for health monitoring, J. Semicond. 44 (2023) 021601, https://doi.org/10.1088/1674-4926/44/2/021601.

[24] Y. Wang, S. Ma, L. Hu, Z. Fan, Y. Lin, Wearable and printable devices for electrolytes sensing, Nano Futures 7 (2023) 032002, https://doi.org/10.1088/2399-1984/ace40e.

[25] A. Kar, N. Ahamad, M. Dewani, L. Awasthi, R. Patil, R. Banerjee, Wearable and implantable devices for drug delivery: applications and challenges, Biomaterials 283 (2022) 121435, https://doi.org/10.1016/j.biomaterials.2022.121435.

[26] S. Chu, Y. Liang, H. Yuan, L. Yu, Q. Liu, W. Peng, Ultranarrow linewidth coupling resonance in flexible plasmonic nanopillar array for enhanced biomolecule detection, Adv Materials Inter 9 (2022) 2201011, https://doi.org/10.1002/admi.202201011.

[27] Q. Hua, G. Shen, A wearable sweat patch for non-invasive and wireless monitoring inflammatory status, J. Semicond. 44 (2023) 100401, https://doi.org/10.1088/1674-4926/44/10/100401.

[28] F. Criscuolo, I. Ny Hanitra, S. Aiassa, I. Taurino, N. Oliva, S. Carrara, G. De Micheli, Wearable multifunctional sweat-sensing system for efficient healthcare monitoring, Sensor. Actuator. B Chem. 328 (2021) 129017, https://doi.org/10.1016/j.snb.2020.129017.

[29] S.Y. Oh, S.Y. Hong, Y.R. Jeong, J. Yun, H. Park, S.W. Jin, G. Lee, J.H. Oh, H. Lee, S.-S. Lee, J.S. Ha, Skin-attachable, stretchable electrochemical sweat sensor for glucose and pH detection, ACS Appl. Mater. Interfaces 10 (2018) 13729–13740, https://doi.org/10.1021/acsami.8b03342.

[30] F. Lorestani, X. Zhang, A.M. Abdullah, X. Xin, Y. Liu, M.M. Rahman, M.A.S. Biswas, B. Li, A. Dutta, Z. Niu, S. Das, S. Barai, K. Wang, H. Cheng, A highly sensitive and long-term stable wearable patch for continuous analysis of biomarkers in sweat, Adv. Funct. Mater. 33 (2023) 2306117, https://doi.org/10.1002/adfm.202306117.

[31] K. Zhou, R. Ding, X. Ma, Y. Lin, Printable and flexible integrated sensing systems for wireless healthcare, Nanoscale 16 (2024) 7264–7286, https://doi.org/10.1039/D3NR06099C.

[32] L. Wang, Y. Luo, Y. Song, X. He, T. Xu, X. Zhang, Hydrogel-functionalized bandages with Janus wettability for efficient unidirectional drug delivery and wound care, ACS Nano 18 (2024) 3468–3479, https://doi.org/10.1021/acsnano.3c10766.

[33] Z. Lv, H. Bao, M. Zhu, Y. Xie, H. Tang, D. Miao, X. Guo, X. Zhai, S. Wang, H. Chen, D. Cong, X. Liu, J. Pei, A novel deformable liposomal hydrogel loaded with a SREBP-1-inhibiting polypeptide for reducing sebum synthesis in golden hamster model, Eur. J. Pharmaceut. Sci. 187 (2023) 106483, https://doi.org/10.1016/j.ejps.2023.106483.

[34] B. Li, B. Qi, Z. Guo, D. Wang, T. Jiao, Recent developments in the application of membrane separation technology and its challenges in oil-water separation: a review, Chemosphere 327 (2023) 138528, https://doi.org/10.1016/j.chemosphere.2023.138528.

[35] M. Zheng, X. Wang, O. Yue, M. Hou, H. Zhang, S. Beyer, A.M. Blocki, Q. Wang, G. Gong, X. Liu, J. Guo, Skin-inspired gelatin-based flexible bio-electronic hydrogel for wound healing promotion and motion sensing, Biomaterials 276 (2021) 121026, https://doi.org/10.1016/j.biomaterials.2021.121026.

[36] J. Yong, Q. Yang, X. Hou, F. Chen, Emerging separation applications of surface superwettability, Nanomaterials 12 (2022) 688, https://doi.org/10.3390/nano12040688.

[37] G.J. Dunderdale, C. Urata, T. Sato, M.W. England, A. Hozumi, Continuous, high-speed, and efficient oil/water separation using meshes with antagonistic wetting properties, ACS Appl. Mater. Interfaces 7 (2015) 18915–18919, https://doi.org/10.1021/acsami.5b06207.

[38] D. Dong, Y. Zhu, W. Fang, M. Ji, A. Wang, S. Gao, H. Lin, R. Huang, J. Jin, Double-defense design of super-anti-fouling membranes for oil/water emulsion separation, Adv Funct Materials 32 (2022) 2113247, https://doi.org/10.1002/adfm.202113247.

[39] M. Yang, N. Sun, X. Lai, J. Wu, L. Wu, X. Zhao, L. Feng, Paper-based sandwich-structured wearable sensor with sebum filtering for continuous detection of sweat pH, ACS Sens. 8 (2023) 176–186, https://doi.org/10.1021/acssensors.2c02016.
[40] Y. Liu, X. Li, H. Yang, P. Zhang, P. Wang, Y. Sun, F. Yang, W. Liu, Y. Li, Y. Tian, S. Qian, S. Chen, H. Cheng, X. Wang, Skin-Interfaced superhydrophobic insensible sweat sensors for evaluating body thermoregulation and skin barrier functions, ACS Nano 17 (2023) 5588–5599, https://doi.org/10.1021/acsnano.2c11267.
[41] Y. Zhang, H. Guo, S. Bong Kim, Y. Wu, D. Ostojich, S. Hyeon Park, X. Wang, Z. Weng, R. Li, A. J Bandodkar, Y. Sekine, J. Choi, S. Xu, S. Quaggin, R. Ghaffari, J. A Rogers, Passive sweat collection and colorimetric analysis of biomarkers relevant to kidney disorders using a soft microfluidic system, Lab Chip 19 (2019) 1545–1555, https://doi.org/10.1039/C9LC00103D.
[42] Z. Liu, W.-Q. Shao, Y. Sun, B.-H. Sun, Scaling law of the one-direction flow characteristics of symmetric Tesla valve, Engineering Applications of Computational Fluid Mechanics 16 (2022) 441–452, https://doi.org/10.1080/19942060.2021.2023648.
[43] P. Zhao, H. Wang, Y. Wang, W. Zhao, M. Han, H. Zhang, A time sequential microfluid sensor with Tesla valve channels, Nano Res. 16 (2023) 11667–11673, https://doi.org/10.1007/s12274-023-5778-8.